

Knuckles that buckle: compliant underactuated limbs with joint hysteresis enable minimalist terrestrial robots

Mingsong Jiang¹, Rongzichen Song² and Nick Gravish¹

Abstract—Underactuated designs of robot limbs can enable these systems to passively adapt their joint configuration in response to external forces. Passive adaptation and reconfiguration can be extremely beneficial in situations where manipulation or locomotion with complex substrates is required. A common design for underactuated systems often involves a single tendon that actuates multiple rotational joints, each with a torsional elastic spring resisting bending. However, a challenge of using those joints for legged locomotion is that limbs typically need to follow a cyclical trajectory so that feet can alternately be engaged in stance and swing phases. Such trajectories present challenges for linearly elastic underactuated limbs. In this paper, we present a new method of underactuated limb design which incorporates hysteretic joints that change their torque response during loading and unloading. A double-jointed underactuated limb with both linear and hysteretic joints can thus be tuned to create a variety of looped trajectories. We fabricate these joints inside a flexible legged robot using a modified laminate based 3D printing method, and the result shows that with passive compliance and a mechanically determined joint sequence, a 2-legged minimalist robot can successfully walk through a confined channel over uneven substrates.

I. INTRODUCTION

Underactuation is a widely used design concept in many robotic systems [1], [2], [3], [4]. The number of control inputs (actuators) of an underactuated robot is less than the degree of freedom (DOF) of the system, leading to a reduction of both control and hardware complexity [5]. In the last few decades, we have seen an increased interest in the design of compliant robotic systems exploiting underactuation such as, robotic hands [6], grippers [7], [8] and exoskeletons [9], and walking robots [10], [11], most of which were based on tendon-driven mechanisms enabling lightweight, compact and more energy efficient system designs [12]. The dexterity of the prescribed systems can also be enhanced by their passive adaptability to the unknown environments and more robustness in handling external disturbances.

Oversimplification of an underactuated system does pose constraints for its motion capabilities. For instance, within the simplest tendon-driven underactuated system, where a single tendon actuates in a static equilibrium of a series of rotational joints, the motion sequence of all joints will be predetermined based on each joint's stiffness and the tendon's stress state. This will cause the end effector to follow the exact same path during the loading and unloading half cycle, which can hardly be used to generate legged

MJ¹ and NG¹ are with Department of Mechanical and Aerospace Engineering. RS² is with the department of Electrical and Computer Engineering. All authors are at the University of California San Diego, 9500 Gilman Dr, La Jolla, CA 92093 USA ngravish@eng.ucsd.edu
 (Corresponding author: Nick Gravish)

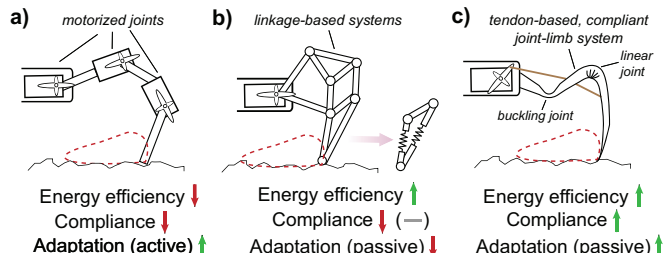


Fig. 1. Comparison between different driving methods to achieve the same cyclical foot trajectory of a robotic leg. a) Redundant actuation by coordinating several motorized joints for the designated foot trajectory. b) Single motor actuation of a series of rigid or semi-compliant linkages to generate the designated foot trajectory. c) A compliant joint-limb system driven by a single tendon actuator to follow the same looped trajectory.

locomotion with hysteretic (or looped) foot trajectories as depicted in Fig. 1. Adding more actuators might solve the problem, however this is at the expense of additional control complexity and energy loss due to the added mass and extra actuators (Fig. 1a). As a simpler design, using a planar linkage mechanism for the leg can reduce the number of actuators to a single revolving input [13], [14]; however, such linkage-based systems can be bulky, challenging to design [15], [16], and inflexible due to the interconnected rigid linkages (Fig. 1b). Although compliant flexures can be used to replace mechanical joints in such systems [17], the overall design concept focuses on creating fixed trajectories with linkage transmissions, which lacks adaptability for different working conditions. In this paper, we present a design concept featuring an underactuated compliant leg system with hysteretic foot trajectories based on a single tendon input. The key of this method relies on the incorporation of joints with nonlinear hysteretic dynamics (hysteretic load-displacement relationship) that can alter the joint motion sequence between loading and unloading cycles. As shown in Fig. 1c, a robot consisting of a prescribed buckling joint coupled with a linear joint can generate a hysteretic loop trajectory based on a single tendon actuator. Among the three leg designs, the compliance is maximized in the tendon-based continuum joint-limb system. Additionally, the energy efficiency can also be improved based on the reduced number of motors and body frames (Fig. 1).

This paper is arranged as follows: we first describe how hysteretic foot trajectories can be achieved from a single tendon actuation via joint hysteresis. A conceptual underactuated leg design is provided which consists of a linear joint in series with a non-linear hysteretic joint based on

snap-through buckling. All joints and limbs are fabricated based on a modified 3D printing process called flexoskeleton printing [18], in which rigid filaments are directly deposited onto a flexible backing to create structures with variable stiffness and complex morphology. The design metrics of the hysteretic joint are explored in detail with a library of joint parameters. By combining a hysteretic buckling joint with a linear bending flexure inside one single leg design, we tracked the hysteretic foot tip trajectories that can be computed based on the principle of minimum (potential) energy. By tracing a designated looped trajectory, we compare the energy cost for driving a single-tendon based hysteretic leg with one that has fully actuated joints. Improvements of the long term durability of a printed flexure can be achieved by incorporating superelastic elements into the deposited layers. Finally, we demonstrate that a compliant underactuated terrestrial robot with prescribed joints can successfully crawl over uneven terrains with hysteretic foot trajectories which can be adapted to navigate through a confined channel based on the same control input and walking substrate.

II. DESIGN & FABRICATION

A. Hysteretic Leg Trajectories via Joint Hysteresis

Joint hysteresis can be defined as a loss of either bending stiffness or elastic energy of a rotational joint when the exerted load exceeds a certain threshold [19], [20]. Such a joint will maintain its low stiffness state as the load releases. This provides opportunities for energy dissipation and overload protection as shown in many biological systems [21]. Alternatively, such a non-linear hysteretic joint behavior can also be utilized to create joint motion sequences with hysteretic end tip trajectories inside a multi-jointed underactuated system. Specifically, under slow actuation, the motion sequence of a single tendon-driven underactuated system is determined by the joint stiffnesses and the tendon displacement. As the displacement increases and reaches the critical load of the hysteretic joint, a sudden drop of load can be observed due to the joint hysteresis thus changing the stiffness during unloading. The whole process is also reflected by the trajectory of the end tip, which will follow a different path during the unloading process as compared with its loading process.

Such a joint mechanism can be illustrated based on a single-tendon driven underactuated robot leg with two rotational joints in series. As shown in Fig. 2a, a leg with two linear joints will not generate a hysteretic foot trajectory due to the symmetric joint dynamics (torque-displacement curve) between loading and unloading. As we introduce joint hysteresis into one of the joints, the joint will then exhibit a lowered extension rate (due to a loss of bending stiffness) as the tendon releases which alters the joint motion sequence. This helps to achieve a hysteretic foot tip trajectory, such as the swing-stance cycle of legged locomotion (Fig. 2b). In this paper, we propose a design concept, the hysteretic buckling joint, or buckling joint, featuring the snap-through buckling of an elastic thermoplastic layer to create the joint hysteresis phenomenon. The joint is a multi-layered bending flexure

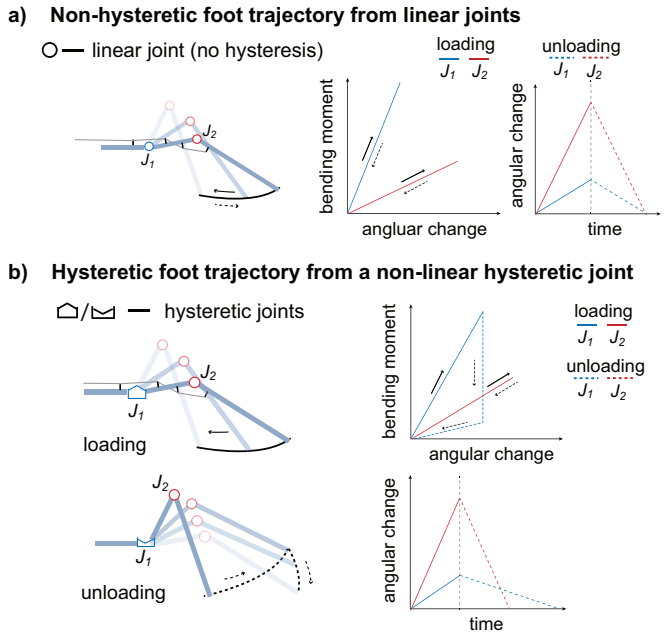


Fig. 2. Illustration of non-hysteretic and hysteretic foot trajectories of a single-tendon, double-jointed robot leg with different joint combinations. a) Non-hysteretic foot trajectory generated from pulling on a series of two linear joints with no joint hysteresis. b) Hysteretic foot trajectory achieved from replacing one of the joint with a hysteretic joint. Hysteretic joints are defined as a loss of bending moment at a certain load threshold. Here the time axis in the plot indicates a displacement control of the tendon.

that can be easily fabricated by using a laminate based 3D printing method. We then explore the joint dynamics as well as the corresponding leg motion by choosing different joint parameters. Note that other methods such as a differential loading-unloading speed, and asymmetric joint frictions during loading-unloading cycles can also lead to a hysteretic foot tip trajectory. However, utilizing joint hysteresis will allow a broader operational spectrum of underactuated legged robots independent of the input speed or frequency.

B. Robot Fabrication using Flexoskeleton Printing

Fabrication of the whole leg design is based on a low cost, laminate inspired 3D printing technique, called: flexoskeleton printing [18]. Here we modify the tradition FDM (Fused Deposition Modeling) printing process to deposit rigid filament directly onto a heated thermoplastic base layer which provides extremely strong bonding strength between deposited material and the inextensible, flexible base layer (Fig. 3a). This process can significantly improve the fatigue resistance of thin-walled flexures printed from rigid filaments and can enable a wide variety rigid morphologies, such as joint limits that can be jammed at an extreme bending curvature (Fig. 3c). To improve the material properties, a pause and place step can be introduced by embedding functional elements into the printed structures. For instance, we add superelastic nitinol fibers inside flexoskeleton joints to increase the elastic recovery of the joint under large deflections.

The “hysteretic buckling joint (or buckling joint)”, is fabricated based on flexoskeleton printing and embedded into

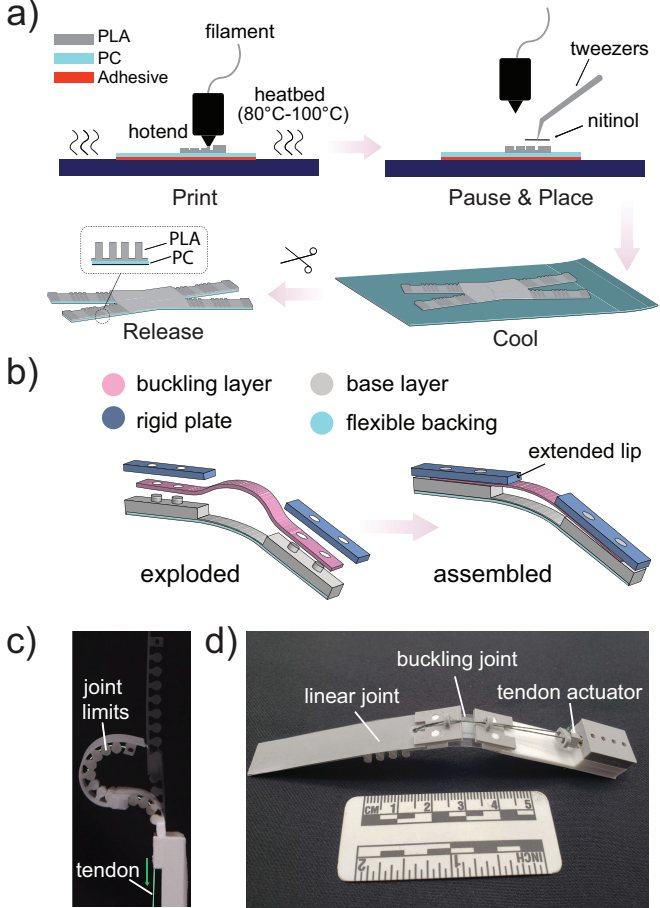


Fig. 3. Fabrication of a hysteretic buckling joint based on flexoskeleton printing. a) General process of flexoskeleton printing [18]. b) Material composition of a buckling joint with a constrained (snap-through) buckling layer. c) A compliant bending structure with joint limits printed for locking at extreme bending curvatures. d) An assembled underactuated leg with one linear joint and one hysteretic buckling joint controlled by a single tendon actuator.

a multi-layered hinge structure with three main components: a) A base layer with a soft hinge (0.1 mm–0.2 mm PC + 0.1 mm–0.3 mm PLA) bridging two adjacent rigid offsets. b) A middle buckling layer (PC film, 0.1 mm–0.2 mm) longer than the base hinge stacked between the rigid components. c) Printed top plates with extended lips to exert force onto the pre-curved buckling layer which causes the initial snap-through motion. Such a joint will exhibit a pre-curved geometry at its neutral state due to the relatively longer buckling layer (Fig. 3b).

A simple underactuated hysteretic leg design we proposed in this paper is composed of one linear joint and one buckling joint controlled by a single tendon actuator. Fig. 3d shows a 3D printed leg prototype, with a buckling joint placed on the proximal end of the leg. This helps to generate front leg pulling motion as will be explained in the result section. Depending on the design scales and requirements for extra load support, either a servo or DC motor with (twisted) strings can be used for powering the motion cycles. Each leg takes 20 min–30 min to fabricate with its length ranging

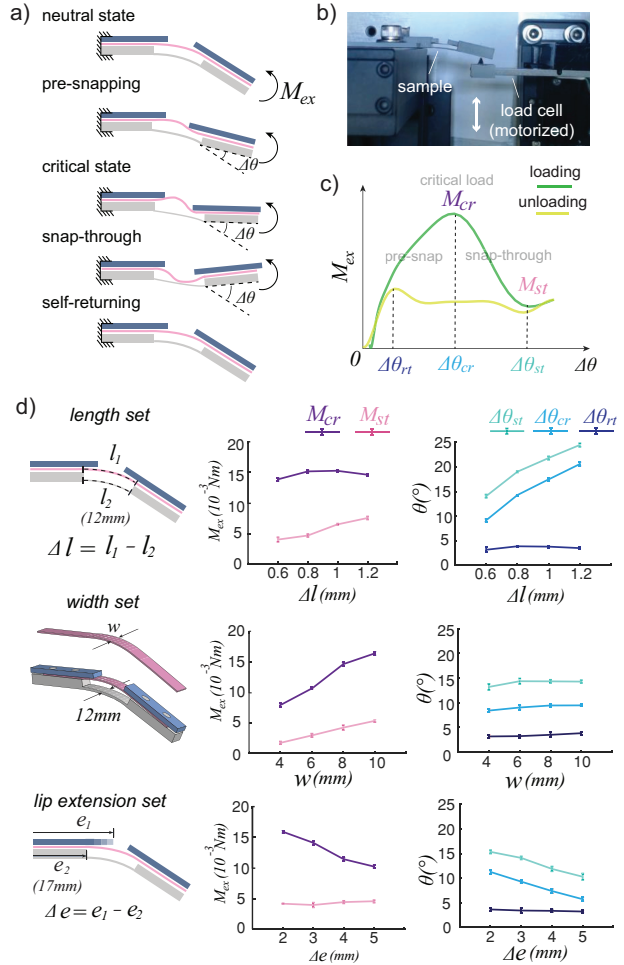


Fig. 4. Parametric study of the buckling joints. a) Different states of a buckling joint under external bending moment M_{ex} during a loading-unloading cycle. $\Delta\theta$, the joint angular displacement is defined as the change of the distal beam orientation. b) Experimental setup for the bending test. c) A torque-displacement curve of a buckling joint during loading-unloading cycle. To simplify the joint hysteresis, five key hysteretic joint parameters are summarized: M_{cr} , the critical bending moment, M_{st} , the stabilized bending moment after layer snap-through, $\Delta\theta_{cr}$, angular displacement at the critical state, $\Delta\theta_{st}$, angular displacement at the snap-through state, $\Delta\theta_{rt}$, angular displacement when the joint starts to return to its neutral state (a baseline parameter). d) An exploration of the hysteretic joint parameters by changing the geometric design of the buckling joint. Each data point is averaged over five individual samples with the error bar representing one standard deviation.

from 40 mm–80 mm, and its weight from 1 g–3 g. The resolution of all the prints are 0.1mm as we use a 0.25mm nozzle size for material deposition.

III. RESULTS & DISCUSSIONS

A. Parametric Study of the Hysteretic Buckling Joint

Joint hysteresis can be achieved from snap-through buckling of an elastic beam or layer. As shown in Fig. 4a, a buckling joint is pre-curved by a buckling layer (pink) constrained inside a joint chassis. The key states of a buckling joint undergoing a nonlinear bending and buckling motion can be characterized as: 1) neutral state, where the buckling layer is pre-curved due to the length effect; 2)

pre-snapping state, as force is induced onto the buckling layer by the extended lip from one rigid plate; 3) critical state, where the exerted load reaches its peak value; 4) snap-through state, as the buckling layer snaps into a buckled shape causing a significant drop of load; 5) self-returning of the buckling layer, which is recovered from the stored elastic energy. The angular displacement $\Delta\theta$ of the buckling joint is characterized as the beam orientation of the distal rigid plate, an approximation of the rotary motion from a flexure-based joint.

The hysteretic joint dynamics are measured based on a cantilever beam bending test. As shown in Fig. 4b, the buckling joint is fixed on a stationary stage with a load cell (lbb200, 1 lb, FUTEK) driven by a linear motorized stage (Thorlabs, MTS25-Z8). The load cell is displaced at a speed of 2 mm/s. The joint angular displacement is measured based on a digital camera where we measure the moment arm based on image processing and convert the measured force into torque. A typical torque-displacement curvature of a buckling joint is plotted in Fig. 4c. Here we choose five key parameters to characterize the hysteretic torque-displacement relationship: M_{cr} , the critical bending moment, M_{st} , the stabilized bending moment after the snap-through motion, $\Delta\theta_{cr}$, joint angular displacement at the critical state, $\Delta\theta_{st}$, joint angular displacement at the snap-through state, $\Delta\theta_{rt}$, joint angular displacement when the joint starts to return to its neutral state.

Each joint sample is fabricated with 44 mm–46 mm long and 12mm wide, with a 0.2 mm thickness for the middle layer, and 2 mm for both the base layer offsets. The soft hinge of the base layer is composed by 0.1 mm PC and 0.2 mm printed PLA. From the parametric study (Fig. 4d) we can observe that lengthening the middle buckling layer l_1 relative to the base hinge l_2 (12 mm) will increase the post snap-through bending moment with little change in the critical load. Since a longer middle layer means a more pre-curved shape before bending, the effective range for the joint hysteresis operation can be increased by having a longer middle buckling layer. On the other hand, changing the width of the middle buckling region will not affect the pre-curved shape of the joint and thus the operational range (Fig. 4d middle row, right). However, we do observe a linear increase of both M_{cr} and M_{st} as we increase the width of the middle buckling layer, showing a strengthening effect of the overall buckling difficulty. This is largely due to the increased flexural strength of the buckling layer which should have similar effects if we increase the thickness of the buckling layer. Lastly, considering the extended rigid lip which is in direct contact with the middle buckling layer, different force locations might affect the bending dynamics of the buckling joint according to a lot of research [22], [23], [24]. As shown in Fig. 4d bottom row, increasing the extensional length of the rigid lip will decrease the critical load required for the snapping motion, with a shortened operational range for joint hysteresis. This means that a transitional force location close to the central axis of the buckling layer lowers the snap-through requirement and lessens the pre-curving energy

accumulated from the pre snap-through state.

B. Tracking and simulation of Hysteretic Leg Trajectories

The motion of serial joints (linear and nonlinear) actuated slowly by a single tendon actuation can be computed from the principle of minimum energy. The total potential energy of the system E_{sys} can be represented as the addition of both the elastic energy E_e , stored inside the joints and the gravitational energy E_g based on the body mass distribution, as shown in (1) and Fig. 5a. As the tendon varies in length, the joint kinematics θ_1 and θ_2 should be solved based on the minimization of E_{sys} for different values of tendon length, which can be further converted into foot tip trajectories. The simulation of the leg trajectory is based on the use of a MATLAB function, ‘fmincon’, to find the minimized pair (θ_1, θ_2) with constraints on joint limits under infinitesimal tendon variation.

$$E_{sys} = E_e + E_g \quad (1)$$

Experimental validation of the foot trajectories are conducted based on a double-jointed underactuated leg system that can pull on the substrate and relocate its foot tip as a hysteretic motion cycle. As shown in Fig. 5b, J_2 will bend first due to its lower stiffness which pulls the foot tip towards the ground and further drags it towards the robot (Fig. 5b(1-3)). As the tendon continues pulling with J_2 already locked up by the joint limits ($\theta_{2max}=78^\circ$ and $\theta_{1max}=38^\circ$), J_1 will start to bend and makes a sudden change of angle due to the snap-through motion as well as the sudden release of the elastic energy. This is the point where the tendon stops pulling as both joints reach their joint limits. However, as the tendon releases, the linear joint will start to flex back together with the buckling joint due to a loss of bending stiffness in J_1 (whose order should be J_1 first and then J_2 if both are linear joints), which creates the hysteretic tip motion as shown in Fig. 5b(6).

As to compare between trajectories with different joint combinations, we fabricate linear joints with different thickness (stiffness): 0.2 mm PLA+0.1 mm PC, 0.3 mm PLA + 0.1 mm PC, and 0.4 mm PLA + 0.1 mm PC. Different foot tip trajectories are tracked and predicted based on the principle of minimum system energy with measured joint dynamics (from the bending test). The results are shown with a highlight of the maximum stroke and lift distance for a successful hysteretic trajectory (Fig. 5c). It can be observed that the stiffness of J_2 (linear joint) has an important role in determining the shape of the hysteretic trajectory. With low stiffness J_2 , the foot will not generate a hysteretic foot trajectory as the joint is still too soft compared with an already snapped buckling joint J_1 . However, by increasing the stiffness of the linear joint, successful looped trajectories can be achieved with increased lift height (y_{max}) and reduced drag distance (x_{max}) through a stiffer linear joint. The buckling joint in this set has the same design parameters with the ones in Section III(A), with $\Delta l=0.6$ mm, $w=8$ mm and $\Delta e=3$ mm. To further test, we change the length of

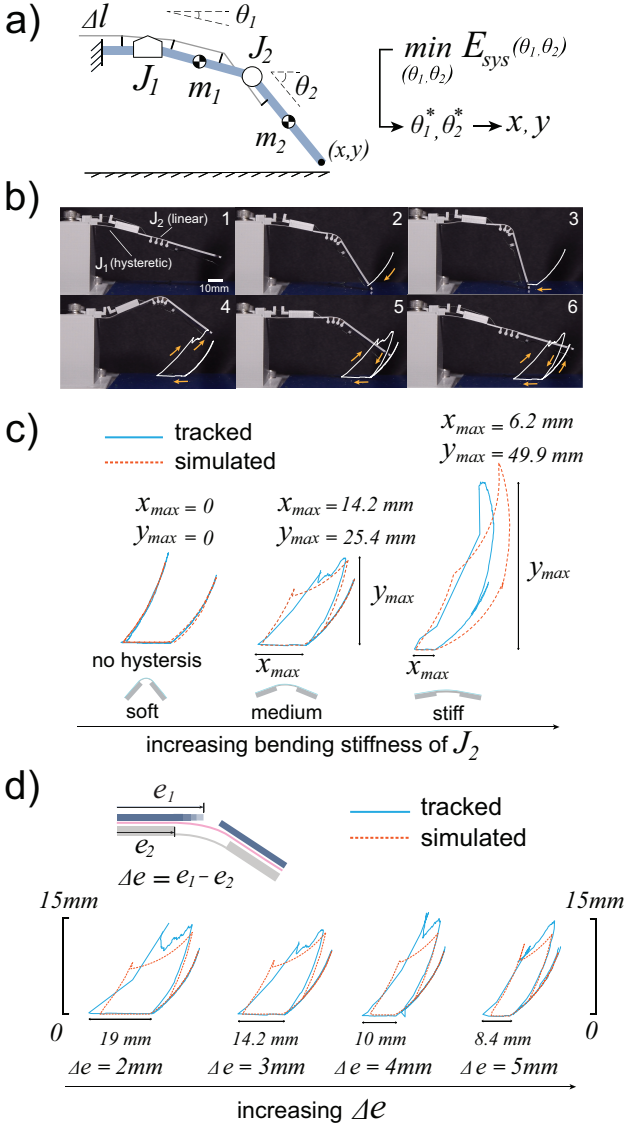


Fig. 5. Tracking and simulation of the limb trajectories under different joint dynamics a) Solving the joint kinematics based on the minimum of the system energy E_{sys} . b) Step-by-step hysteretic leg motions based on a linear and hysteretic joint with a single tendon input. c) Tracking of different leg trajectories by varying the joint stiffness of J_2 (linear joint). d) Tracking of different leg trajectories by changing the length of the extended lip of J_1 (buckling joint).

the extended rigid lip Δe , with the same linear joint J_2 (medium stiffness). As shown in Fig. 6d, by increasing Δe , we observe a shortened horizontal stroke distance due to decreased critical loads (Fig. 4d) and a relatively unchanged lift height due to the variable joint limits of J_1 . This draws different conclusions from the stiffness set and further shows that tuning the joint dynamics will enable a range of programmable foot trajectories.

C. Energy Consumption of a Hysteretic Leg System

The energy consumption of a fully actuated, multi-DOF robot has always been a concern due to extra motor mass and the computational cost from coordinating multiple joints based on sensory feedback [25]. Simplifying joint motions

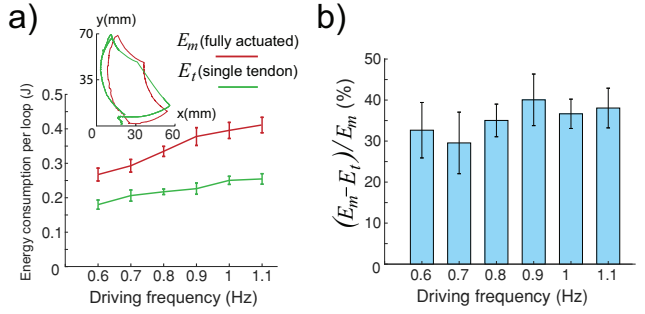


Fig. 6. Comparison of energy consumption between a fully actuated leg with a single tendon driven underactuated leg. a) Energy consumption per loop cycle over different driving frequencies. b) Energy reduction from the underactuated limb over the fully actuated limb under each driving frequency. Each data point is averaged over 10 individual measurements, with the error bar represents one standard deviation.

by pre-programming the motion sequence and reducing the number of actuators using underactuation might reduce the total energy cost without sacrificing the kinematic capabilities. In this section, we compare the energy consumption between a double-jointed, fully actuated robotic leg with our single-tendon driven hysteretic leg based on similar leg geometry and trajectory. To reduce uncertain loads and noises, both legs are fixed at a stationary stage with their foot tip tracing a similar looped cycle as shown in Fig. 6a. The energy consumption is measured by the integration of the power output across the motors (Tower Pro, SG92R), which is measured from the current flow using a current sensor (INA219) and the corresponding voltage output using a DAQ (NI USB-6009) over the entire motion cycle. We then repeat the same experiment over a range of driving frequencies (from 0.6 to 1.1 Hz). It can be seen that the energy consumption will increase as we increase the driving frequency for both cases. However, on average the underactuated leg will consume 30–40% less energy than the fully motorized leg. Although the comparison set is not conducted on a real walking robot, we believe that with added mass from one extra motor (11.6g compared with 3g for the leg), the extra energy required for working against the gravity will not be trivial on the fully actuated robot leg.

D. Bending Fatigue and Improvements

One critical challenge facing 3D printed components from standard filaments is the low fatigue resistance [26], [27]. Previous work [18] has shown that printing thin-walled structures onto a flexible backing will increase the fatigue resistance. As a further improvement, we embed superelastic nitinol fibers (0.25 mm–0.5 mm in diameter) inside our bending flexures based on a pause and place fabrication step (Fig. 3a). We then compare the creep angle between flexures with and without nitinol fibers under cyclic loads. The experiments are done by using a L-shaped rigid deflection paddle to apply stress from one side of the sample (Fig. 7a). All samples are designed with the same geometry: 32 mm x 22 mm x (0.2 mm PLA + 0.1 mm PC) with a 0.5 mm in diameter nitinol added lengthwise in the middle

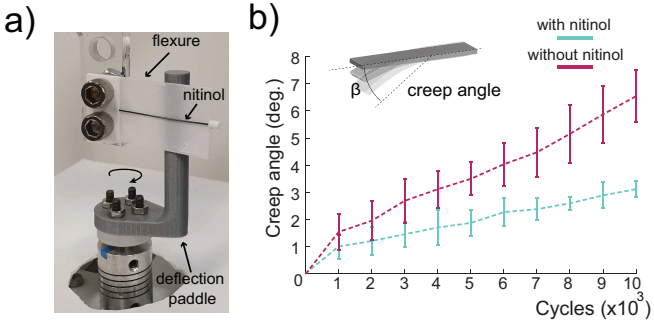


Fig. 7. Comparison of the fatigue resistance between materials with and without nitinol reinforcement. a) Experimental setup for testing the fatigue resistance of a bending flexure. b) Creep angles measured from two types of bending flexures over increasing load cycles. Each data point is averaged over five individual samples with the error bar represents one standard deviation. The maximum of the applied stress is maintained constant among all testing samples.

of the flexure. The maximum stress applied to all samples is maintained constant with a maximum bending angle of 26.9° with nitinol and 35.8° without nitinol. The result (Fig. 7b) shows that for both cases, the creep angle will increase linearly with increasing load cycles. However, the flexure with nitinol embedded will have a significantly lessened (about half) creep angle compared with the one without nitinol reinforcement. This method provides insights for improving the material properties of current flexoskeleton printed components (e.g. joints and flexures) with embeddable, functional elements.

IV. DEMONSTRATIONS

To demonstrate the capabilities of an underactuated robot with the proposed hysteretic legs and joints, we built a two-legged flexoskeleton terrestrial robot with crawling motion over uneven substrates. The robot is designed and assembled using all flexoskeleton printed limbs and chassis with each leg driven by a single tendon actuator (Tower Pro, SG92R plus fishing wire) as shown in Fig. 8a. Each leg is composed of one hysteretic joint and one linear joint and is programmed to generate alternating foot steps between the left and right limb (180° phase difference). The whole robot weighs about 30 g, with its size of 76 mm x 43 mm x 34 mm (L x W x H). An uneven substrate is fabricated by using an acrylic sheet with cut grooves as individual steps (Fig. 8b). Thus the robot has to relocate its foot to lift over the grooves in order to move forward, requiring a hysteretic foot trajectory that enable forward motion despite low friction from the feet. For robot walking on such a terrain without vertical confinement, the walking speed is 50 mm/s or 0.7 body length/s. To highlight the passive adaptability from the compliant and continuum limb structures, we operate the robot inside a confined channel (height: 45.7 mm), with its vertical range compressed by a small amount (naturally about 55.4 mm when one leg is fully lifted). In this case, the robot could still perform steady crawling motion at 10.6 mm/s or 0.2 body length/s with the same driving inputs. Unlike traditional rigid linkage based robots, limb compliance from our

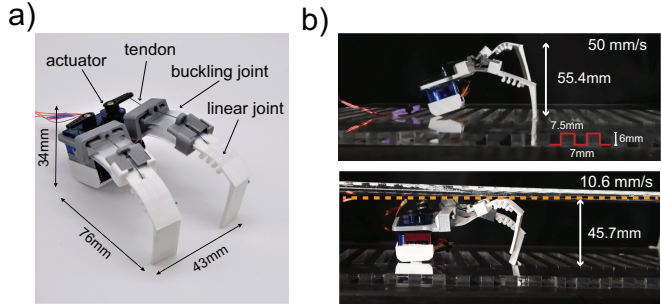


Fig. 8. A two-legged crawling robot and its performances under different environments. a) A prototype of the crawling robot with flexoskeleton printed limbs and chassis. b) Crawling on an uneven substrate with and without vertical confinements. The speed is averaged over the whole distance (290mm). The geometry of the cut grooves is shown in the picture.

underactuated tendon-based hysteretic leg system is critical for a) overload protection as we use the same torque input and b) passively adaptable limb kinematics to suit different environments such as a confined channel without the need to switch any robot components.

V. CONCLUSIONS

This paper presents a buckling-based approach to achieve hysteretic foot trajectories of a compliant, underactuated terrestrial robot based on a single tendon input. The key of this method relies on the incorporation of joint hysteresis into the leg design which is based on the snap-through buckling of layered hinges independent of the driving conditions. The whole robot (including hysteretic joints and legs) can be fabricated using a modified 3D printing technique, called flexoskeleton printing, where we embed superelastic elements to improve the long-term bending performance of the printed components. An exploration of the joint parameters indicates a library of joint hysteretic dynamics which can be used to program the leg trajectories as we combine one hysteretic joint with a linear joint inside one underactuated leg design. Due to the reduced number of actuators, the energy consumption for the underactuated leg design will be significantly lowered compared to a fully actuated leg design. Ultimately, the hysteretic leg motion is incorporated into an underactuated crawling robot with passive compliance to navigate through either an open space or confined channel over uneven substrates.

One main concern for our robot design is it lacks the ability to generate different trajectories while being operated compared to a fully actuated walking robot. However, considering the coordination between multiple actuators through feedback control as well as the added mass of a fully actuated system, we argue that a light weight, underactuated robot with passively compliant limbs may be capable of adapting to many different walking conditions. In future robot designs, we see opportunities for tight design coordination between non-linear mechanical properties of joints and single DOF actuation strategies.

ACKNOWLEDGMENT

Funding support was provided through the Mechanical and Aerospace Engineering Department at UCSD. This material is based upon work supported by the National Science Foundation under Grant No. 1935324. Any opinions, findings, and conclusions or recommendations expressed in this material are those of the author(s) and do not necessarily reflect the views of the National Science Foundation.

REFERENCES

- [1] Bin He, Shuai Wang, and Yongjia Liu. Underactuated robotics: a review. *International Journal of Advanced Robotic Systems*, 16(4):1729881419862164, 2019.
- [2] Reza Olfati-Saber. *Nonlinear control of underactuated mechanical systems with application to robotics and aerospace vehicles*. PhD thesis, Massachusetts Institute of Technology, 2001.
- [3] Thierry Laliberte, Lionel Birglen, and Clement Gosselin. Underactuation in robotic grasping hands. *Machine Intelligence & Robotic Control*, 4(3):1–11, 2002.
- [4] Mark W Spong. Underactuated mechanical systems. In *Control Problems in Robotics and Automation*, pages 135–150. Springer Berlin Heidelberg, 1998.
- [5] Ramiro Cabás, Luis María Cabas, and Carlos Balaguer. Optimized design of the underactuated robotic hand. In *Proceedings 2006 IEEE International Conference on Robotics and Automation, 2006. ICRA 2006.*, pages 982–987. IEEE, 2006.
- [6] Lionel Birglen, Thierry Laliberté, and Clément Gosselin. *Underactuated Robotic Hands*. Springer, Berlin, Heidelberg, 2008.
- [7] Raymond R Ma, Adam Spiers, and Aaron M Dollar. M2 gripper: Extending the dexterity of a simple, underactuated gripper. In *Advances in Reconfigurable Mechanisms and Robots II*, pages 795–805. Springer International Publishing, 2016.
- [8] Serge Montambault and Clément M Gosselin. Analysis of underactuated mechanical grippers. *J. Mech. Des.*, 123(3):367–374, September 2001.
- [9] C J Walsh, D Paluska, K Pasch, W Grand, A Valiente, and H Herr. Development of a lightweight, underactuated exoskeleton for load-carrying augmentation. In *Proceedings 2006 IEEE International Conference on Robotics and Automation, 2006. ICRA 2006.*, pages 3485–3491. ieeexplore.ieee.org, May 2006.
- [10] Oren Y Kanner and Aaron M Dollar. Optimization of coupling ratio and kinematics of an underactuated robot leg for passive terrain adaptability. In *ASME 2012 International Design Engineering Technical Conferences and Computers and Information in Engineering Conference*, pages 1051–1058. American Society of Mechanical Engineers Digital Collection, September 2013.
- [11] Oren Y Kanner and Aaron M Dollar. Kinematic design of an underactuated robot leg for passive terrain adaptability and stability. *J. Mech. Robot.*, 5(3), August 2013.
- [12] R Ozawa, K Hashirii, and H Kobayashi. Design and control of underactuated tendon-driven mechanisms. In *2009 IEEE International Conference on Robotics and Automation*, pages 1522–1527. ieeexplore.ieee.org, May 2009.
- [13] Shivamanappa G Desai, Anandkumar R Annigeri, and A TimmanaGouda. Analysis of a new single degree-of-freedom eight link leg mechanism for walking machine. *Mechanism and Machine Theory*, 140:747–764, 2019.
- [14] Sun-Wook Kim and Dong-Hun Kim. Kinematic analysis of a legged walking robot based on four-bar linkage and jansen mechanism. *Journal of Korean Institute of Intelligent Systems*, 21(2):159–164, 2011.
- [15] Bernhard Thomaszewski, Stelian Coros, Damien Gauge, Vittorio Megaro, Eitan Grinspun, and Markus Gross. Computational design of linkage-based characters. *ACM Trans. Graph.*, 33(4):1–9, 2014.
- [16] Joseph Edward Shigley. *Kinematic analysis of mechanisms*. McGraw-Hill, 1959.
- [17] Anthony DeMario and Jianguo Zhao. A miniature, 3d-printed, walking robot with soft joints. In *International Design Engineering Technical Conferences and Computers and Information in Engineering Conference*, volume 58189, page V05BT08A025. American Society of Mechanical Engineers, 2017.
- [18] Mingsong Jiang, Ziyi Zhou, and Nicholas Gravish. Flexoskeleton printing enables versatile fabrication of hybrid soft and rigid robots. *Soft Robotics*, 2020.
- [19] Animangsu Ghatak, Abhijit Majumder, and Rajendra Kumar. Hysteresis of soft joints embedded with fluid-filled microchannels. *Journal of The Royal Society Interface*, 6(31):203–208, 2009.
- [20] Hans-Theo Weiler and Friedemann Awiszus. Influence of hysteresis on joint position sense in the human knee joint. *Experimental brain research*, 135(2):215–221, 2000.
- [21] Mountcastle Andrew M., Helbling E. Farrell, and Wood Robert J. An insect-inspired collapsible wing hinge dampens collision-induced body rotation rates in a microrobot. *J. R. Soc. Interface*, 16(150):20180618, January 2019.
- [22] Nakul Prabhakar Bende, Arthur A Evans, Sarah Innes-Gold, Luis A Marin, Itai Cohen, Ryan C Hayward, and Christian D Santangelo. Geometrically controlled snapping transitions in shells with curved creases. *Proc. Natl. Acad. Sci. U. S. A.*, 112(36):11175–11180, September 2015.
- [23] W Gronenberg. Fast actions in small animals: springs and click mechanisms. *Journal of Comparative Physiology A*, 178(6):727–734, June 1996.
- [24] A Pandey, D E Moulton, D Vella, and D P Holmes. Dynamics of snapping beams and jumping poppers. *EPL*, 105(2):24001, February 2014.
- [25] Bo Jin, Cheng Chen, and Wei Li. Power consumption optimization for a hexapod walking robot. *Journal of Intelligent & Robotic Systems*, 71(2):195–209, 2013.
- [26] Todd Letcher and Megan Waytashek. Material property testing of 3d-printed specimen in pla on an entry-level 3d printer. In *ASME International Mechanical Engineering Congress and Exposition*, volume 46438, page V02AT02A014. American Society of Mechanical Engineers, 2014.
- [27] OH Ezeh and L Susmel. On the fatigue strength of 3d-printed polylactide (pla). *Procedia Structural Integrity*, 9:29–36, 2018.